RESEARCH ARTICLE

Quantitative Disruption of the NET–ACPA–IL-6 Autoimmune Amplification Loop by Anti-NETotic Agents in Collagen-induced Arthritis

Ahmed Shandookh Hameed*, Wafaa Sadoon Shani

Biology Department, Faculty of Science, Basrah University, Qarmat Ali, Basrah 61004, Iraq

*Corresponding author. Email: ahmedalsaidi@stu.edu.iq

Received date: May 29, 2025; Revised date: Oct 7, 2025; Accepted date: Oct 19, 2025

Abstract

BACKGROUND: Rheumathoid arthritis (RA) is a condition characterized by inflammation of joint lining, which leads to joint destruction and loss of function. Neutrophil extracellular traps (NETs), anti-citrullinated protein antibodies (ACPAs), and interleukin (IL)-6 have been determined to play key roles in development and progression of RA. NETs may trigger citrullination and autoantigen exposure that can lead to ACPA production, while IL-6 increases tissue damage and inflammatory responses. This linked pathway suggests an autoimmune amplification network, but their relationship with disease progression and severity remains unclear. Therefore, this study was conducted to evaluate the relationship of this pathway in collagen-induced arthritis (CIA) mice.

METHODS: Male albino mice were randomly divided into six groups, comprised of healthy control, acute CIA, chronic untreated CIA, and CIA treated with either Myricetin, RL6, or CI-amidine. Levels of serum myeloperoxidase (MPO)-DNA, neutrophil elastase (NE)-DNA, citrullinated histone H3–neutrophil elastase complexes (CitH3–NE), IL-6, IL-1β, tumor necrosis factor-alpha (TNF-α), and ACPAs were determined using enzyme-linked immunosorbent assay (ELISA). These parameters were then statistically analyzed.

RESULTS: Untreated chronic CIA resulted in the highest level of ACPA (81.87±6.17 ng/mL) and had the strongest positive correlation between IL-6 and ACPAs ($r=0.74$, $p<0.001$). All treatments normalized CitH3–NE levels. Myricetin was the most effective in reducing TNF-α by 88.4% and abolishing the significant IL-6–ACPA correlation. This indicated a substantial reduction in the association between inflammatory and autoimmune biomarkers.

CONCLUSION: The results demonstrate a NET–ACPA–IL-6 amplification network in CIA and provide quantitative evidence for anti-NETotic therapies that can differentially dismantle this network. Correlation-network profiling may be a novel pharmacodynamic approach for the assessment of therapeutic efficacy in RA.

KEYWORDS: neutrophil extracellular traps, NETosis, anti-citrullinated protein antibodies, IL-6, collagen-induced arthritis, PAD4 inhibition, MPO inhibition

Indones Biomed J. 2026; 18(5): 438-48

Introduction

Rheumatoid arthritis (RA) is a chronic systemic autoimmune disease affecting approximately 1% of the global population worldwide, with significant morbidity, disability, and socioeconomic burden.(1-3) The disease is characterised by progressive synovial inflammation, cartilage destruction, and bone erosion driven by the interplay of innate and adaptive immune pathways.(4,5) Central to RA pathogenesis is a self-amplifying autoimmune cascade involving the interconnected actions of neutrophil extracellular traps (NETs), anti-citrullinated protein antibodies (ACPAs), and pro-inflammatory cytokines, particularly interleukin (IL)-6.

Among these components, ACPA is a well-established hallmark of RA, with detectable antibodies preceding

Copyright © 2026 The Prodia Education and Research Institute.
This work is licensed under a Creative Commons Attribution-NonCommercial 4.0 International (CC-BY-NC) License.

clinical disease onset by months to years, correlating with disease severity, and predicting radiographic progression.(6,7) However, ACPA production does not occur in isolation; it is closely linked to dysregulated NET formation, which provides a continuous source of citrullinated autoantigens and inflammatory signals. NETs are web-like extracellular structures released by activated neutrophils during NETosis.(8,9) Although NETs serve essential antimicrobial functions under physiological conditions, their excessive or dysregulated formation in autoimmune settings exposes citrullinated self-antigens, thereby promoting ACPA generation and sustaining systemic inflammation.(10,11)

Importantly, the relationship between NETs and ACPA is reciprocal. In the RA synovial microenvironment, NET-derived components can act as danger-associated molecular patterns (DAMPs), activate nucleotide-binding oligomerization domain-like receptor family pyrin domain-containing 3 (NLRP3) inflammasomes, promote ACPA-producing B-cell differentiation, and stimulate fibroblast-like synoviocytes (FLSs) to produce inflammatory mediators, including IL-6.(12,13) Conversely, ACPA-containing immune complexes engage Fcγ receptors on neutrophils, inducing reactive oxygen species (ROS) production and further NET formation.(14) IL-6 provides a critical inflammatory amplification arm within this network by promoting immune-cell activation and sustaining inflammatory responses, while NET-derived products can further enhance IL-6 production by FLSs.(15)

Although the individual contributions of NETs, ACPA, and IL-6 to RA pathogenesis have been increasingly characterised, the strength and dynamics of their interactions have not been systematically quantified as an integrated amplification network. Therefore, defining these interactions may therefore provide a more comprehensive understanding of disease progression and identify the NET–ACPA–IL-6 axis as a potentially measurable and therapeutically modifiable pathogenic network. A large proportion of RA patients continue to suffer from persistent inflammation and progressive joint damage, even with the available therapeutic options, largely because much is still unknown about the basic mechanisms of RA. Hence, it is necessary to identify key pathogenic interactions as well as strategies for disrupting disease-promoting pathways. Collagen-induced arthritis (CIA) model might be able to serve as an appropriate tool for such studies because it shares immunological and pathological features with human RA. Therefore, this study was conducted to evaluate the relationship of NET–ACPA–IL-6 amplification loop pathway in collagen-induced arthritis (CIA) mice.

Methods

Experimental Design and Animals Grouping

One-hundred-and-eighty male albino mice, aged 8–10 weeks and weighing 25–40 g, were obtained from a certified animal facility and housed under standardised conditions (12-hour light/dark cycle; temperature 22±2°C; relative humidity 55±5%; *ad libitum* standard rodent chow and sterile water). Animals were acclimatised for one week before experimental procedures and randomly allocated to groups using a computer-generated random number sequence. Animals were randomly allocated into 6 experimental groups (n=30 per group) as detailed in Table 1. G1 and G2 were sacrificed on day-28 (peak acute CIA), while G3, G4, G5, and G6 were sacrificed on day-49 (established chronic CIA), enabling direct quantitative comparison of the NET–ACPA–IL-6 amplification loop across acute disease, chronic untreated disease, and three weeks of anti-NETotic therapeutic intervention.

CIA Induction Protocol

CIA was established by a two-component simultaneous injection protocol on day-0: 1) intra-articular injection of

Table 1. Experimental groups, CIA induction, treatment allocation, and sacrifice time points (n=30 per group).

Group	Designation	n	CIA Induction	Treatment (Day-28 to -49)	Sacrifice Time
G1	Healthy control	30	None	None	Day-28
G2	Acute CIA	30	Day-0, Day-14	None	Day-28
G3	Chronic untreated CIA	30	Day-0, Day-14	None	Day-49
G4	Chronic CIA + 5 mg/kg/day-Myricetin (p.o.)	30	Day-0, Day-14	Myricetin	Day-49
G5	Chronic CIA + 30 mg/kg/day-RL6 (i.p.)	30	Day-0, Day-14	RL6	Day-49
G6	Chronic CIA + 10 mg/kg 3×/week CI-Amidine (i.p.)	30	Day-0, Day-14	CI-Amidine	Day-49

p.o.: per oral gavage; i.p.: intraperitoneal injection.

10 µL of type II collagen (CII; 2 mg/mL in 0.1 M acetic acid) into the right knee joint using a 29-gauge needle under brief isoflurane anaesthesia; and 2) subcutaneous injection of 100 µL of complete Freund's adjuvant (CFA; supplemented with *Mycobacterium tuberculosis* H37Ra, 4 mg/mL) at the base of the tail. An identical booster was administered on day-14. Disease severity was monitored by a standardised clinical arthritis scoring system (0–4 per paw; maximum 16) every three days from day-7 onwards.

Therapeutic Agents and Administration

Three anti-NETotic agents targeting distinct pathways involved in NET formation were used: Myricetin, targeting myeloperoxidase (MPO) and protein arginine deiminase 4 (PAD4) (16); RL6 (1,8-naphthalimide), a selective MPO inhibitor (17); and CI-Amidine, a selective PAD4 inhibitor (16,18). G1, G2, and G3 received no treatment, whereas G4 received Myricetin (purity ≥98%; Cat. No. M6760; Sigma-Aldrich, St. Louis, MO, USA) by oral gavage at 5 mg/kg/day, dissolved in 0.5% carboxymethylcellulose sodium solution, from day 28 to day 49, G5 received RL6 (purity ≥97%; Sigma-Aldrich) intraperitoneally at 30 mg/kg/day from day 28 to day 49, and G6 received CI-Amidine (purity ≥98%; Cat. No. 10599; Cayman Chemical, Ann Arbor, MI, USA) intraperitoneally at 10 mg/kg three times per week from day 28 to day 49, consistent with previously established PAD4 inhibitor protocols in CIA model.(18)

Sample Collection

At designated sacrifice time points, animals were anaesthetised with 80/10 mg/kg ketamine/xylazine intraperitoneally. Blood was collected via cardiac puncture, serum separated by centrifugation (3,000 rpm, 15 min, 4°C), aliquoted, and stored at −80°C. All samples were analysed within one freeze-thaw cycle. Synovial lavage fluid was collected from the right knee joint using sterile normal saline (0.9% NaCl) for fluorescence microscopy.

Enzyme-linked Immunosorbent Assay (ELISA) Quantification

To measure MPO-DNA, neutrophil elastase (NE)-DNA, citrullinated histone H3-neutrophil elastase (CitH3-NE), IL-6, IL-1β, tumor necrosis factor (TNF)-α, and ACPA levels, ELISA methods were performed using commercially available ELISA as follow: Mouse MPO-DNA (Myeloperoxidase-DNA) Complex ELISA Kit (Cat. No. SG-35905; SinoGeneclon Co., Ltd, Hangzhou City, China), Mouse NE-DNA Complex ELISA Kit (Neutrophil Elastase-DNA Complex) (Cat. No. SG-35904; SinoGeneclon Co., Ltd), Mouse H3cit-NE QuickTest ELISA Kit (Cat. No. QT-EM2516; FineTest, Wuhan, China), Mouse IL-6 ELISA Kit (Cat. No. EM0121; FineTest), Mouse IL-1β ELISA Kit (Cat. No. EM0109; FineTest), Mouse TNF-α ELISA Kit (Cat. No. EM0183; FineTest); and Mouse ACCPA (Anti-Cyclic Citrullinated Peptide Antibody) ELISA Kit (Cat. No. ELK0589; ELK Biotechnology, Wuhan, China). These assays were based on a sandwich ELISA principle in which target analytes bind to specific capture antibodies pre-coated on microplate wells and are detected with enzyme-conjugated secondary antibodies. After the incubation and washing steps to remove unbound materials, tetramethylbenzidine (TMB) substrate was added for color development. The reaction was terminated by the stop solution provided, and the optical density was read at 450 nm with a microplate reader. Standard curves were prepared for each analyte, and their concentrations were calculated. All samples and standards were run in duplicate.

Fluorescence Microscopy for NETosis Detection

Synovial lavage fluid (5–10 µL recovered per joint) was placed on glass slides, stained with 500 nM SYTOX Green nucleic acid stain (Cat. No. S7020; Thermo Fisher Scientific, Waltham, MA, USA) for 15 min at room temperature, protected from light, and examined by fluorescence microscopy at excitation/emission 488/523 nm. NETosis was quantified as the percentage of cells displaying characteristic extracellular web-like chromatin morphology across five random microscopic fields per sample by a blinded observer.

Statistical Analysis

Data were analysed using IBM SPSS Statistics (Version 26; IBM Corp., Armonk, NY, USA). The Shapiro-Wilk test was applied to check the normality of the data. Differences among experimental groups were analysed using one-way analysis of variance (ANOVA) followed by Games-Howell post-hoc comparisons. Pearson's correlation coefficient (r) was separately calculated within each group for all seven measured biomarkers. A probability level of $p<0.05$ was considered significant.

Results

Differential Regulation of Serum NETosis Markers in Experimental Groups

G2 had the highest MPO-DNA (373.32±59.23 ng/mL; letter a), a 21.3-fold elevation above G1 (17.50±3.75 ng/

Table 2. Serum biomarker concentrations across six experimental groups.

Biomarker	G1	G2	G3	G4	G5	G6
MPO-DNA (ng/mL)	17.50±3.75^{f}	373.32±59.23^{a}	227.58±54.64^{b}	43.87±7.84^{d}	59.18±9.13^{e}	57.47±10.34^{e}
NE-DNA (ng/mL)	8.70±2.45^{e}	145.60±19.71^{a}	73.89±10.86^{b}	55.14±9.57^{cd}	66.89±20.52^{bc}	53.40±9.97^{d}
CitH3-NE (ng/mL)	1.12±0.54^{e}	26.84±8.80^{a}	21.54±2.32^{b}	1.07±0.67^{e}	1.85±0.70^{e}	1.17±0.54^{e}
IL-6 (pg/mL)	1.97±0.45^{f}	74.04±14.85^{a}	79.12±7.88^{a}	36.70±3.71^{e}	57.91±16.01^{c}	45.96±5.33^{d}
IL-1β (pg/mL)	29.45±8.13^{e}	84.58±27.12^{a}	84.15±14.08^{a}	59.00±8.92^{c}	75.82±11.65^{ab}	53.20±9.90^{cd}
TNF-α (pg/mL)	6.99±3.46^{e}	225.19±13.51^{a}	217.99±13.99^{a}	26.11±5.66^{d}	64.71±15.87^{c}	64.58±14.16^{c}
ACPA (ng/mL)	6.69±3.32^{e}	74.57±19.60^{b}	81.87±6.17^{a}	44.56±4.85^{c}	51.28±6.13^{d}	40.52±7.64^{c}

Values are presented as mean±SD (n=30 per group). Mean difference between groups was tested with One-way ANOVA followed by Games–Howell post-hoc pairwise comparisons. Within each biomarker row, groups sharing at least one superscript letter are not significantly different from each other (p>0.05), whereas groups with no superscript letters in common are significantly different (p<0.05). Superscript letters were assigned to all groups according to the Games–Howell post-hoc comparison results.

mL; letter f), consistent with the marked spontaneous NETosis propensity documented in RA low-density neutrophils as previously reported.(19) G3 demonstrated partial spontaneous reduction (227.58±54.64; letter b; −38.9% *vs.* G2). G4 achieved the greatest MPO-DNA reduction (43.87±7.84; letter d; 88.2% *vs.* G2); G5 and G6 were statistically equivalent (letter c). For NE-DNA, G6 (53.40±9.97; letter d) outperformed G5 (66.89 ± 20.52; letter bc), confirming PAD4 inhibition as the rate-limiting step for NE nuclear translocation (Table 2, Figure 1). The requirement of MPO for optimal NET formation has been established in innate immunity contexts, supporting the mechanistic rationale for RL6's upstream MPO inhibition in this model.

Altered Serum Levels of TNF-α, IL-6, and IL-1β in Experimental Arthritis Model

TNF-α was statistically equivalent in G2 and G3 (225.19±13.51 and 217.9±13.99pg/mL, respectively; both letter a), confirming the self-perpetuating NET-cytokine feedback loop. G4 achieved an 88.4% TNF-α reduction (26.11±5.66 pg/mL; letter d), the highest cytokine suppression in this study. IL-6 in G3 (79.12±7.88 pg/mL) marginally exceeded G2 (74.04±14.85; both letter a; p>0.05), directly evidencing progressive IL-6 entrenchment in the chronic CIA phase consistent with the specific increase in joint NET-related markers and their relation to IL-6 in autoimmune arthritis reported. The IL-1β hierarchy was diagnostically critical: G5 (75.82±11.65;

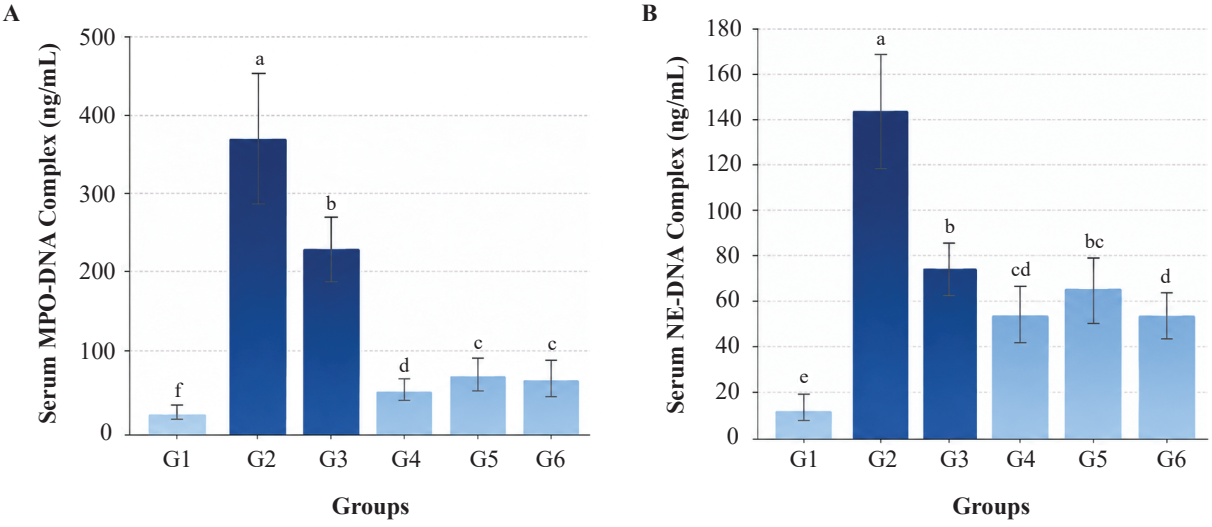


Figure 1. Serum MPO-DNA complex (A) and NE-DNA complex (B) levels across six experimental groups. Values are presented as mean±SD (n=30 per group). Mean difference between groups was tested with One-way ANOVA with Games-Howell post hoc test. Different superscript letters (a–f) indicate statistically distinct groups (p<0.05).

letter ab, not significantly different from G2) achieved substantially less suppression than G4 (59.00±8.92; letter c) and G6 (53.20±9.90; letter cd) despite equivalent CitH3-NE normalisation across all treatment groups (Figure 2), demonstrating that upstream MPO inhibition alone cannot interrupt NLRP3 inflammasome-driven IL-1β production.

Strong Association between Serum CitH3-NE and ACPA Reflecting PAD4-Driven Loop Amplification

CitH3-NE exhibited the highest proportional elevation: G2 (26.84±8.80 ng/mL; 23.96-fold above G1). The convergent finding was complete normalisation of CitH3-NE in all three treatment groups: G4 (1.07±0.67), G5 (1.85±0.70), and G6 (1.17±0.54 ng/mL), all statistically indistinguishable from G1 (1.12±0.54; all letter c). ACPA revealed the most immunologically significant finding: G3 (81.87±6.17; letter a) exceeded G2 (74.57±19.60; letter b), demonstrating progressive autoimmune amplification of 0.34 ng/mL ACPA per day over 21 days, the first quantified NET–ACPA loop velocity in CIA. The progressive ACPA expansion observed in this CIA model is consistent with the ACPA titre increases in early inflammatory arthritis documented longitudinally, further validating the translational relevance of this preclinical amplification rate. G4 and G6 achieved equivalent maximal ACPA reduction (both letter c); G5 demonstrated intermediate suppression (letter d) (Table 2, Figure 3). Citrullinated histones released by NETs are specifically targeted by RA-derived autoantibodies, confirming their central role as ACPA-generating autoantigens.

Comparative Analysis of Serum Biomarkers Across Experimental Groups

Table 2 presents a complete statistical analysis of serum levels of seven biomarkers for the six experimental groups (G1–G6). There were highly significant differences among all the parameters studied (p<0.0001) with One-way ANOVA,

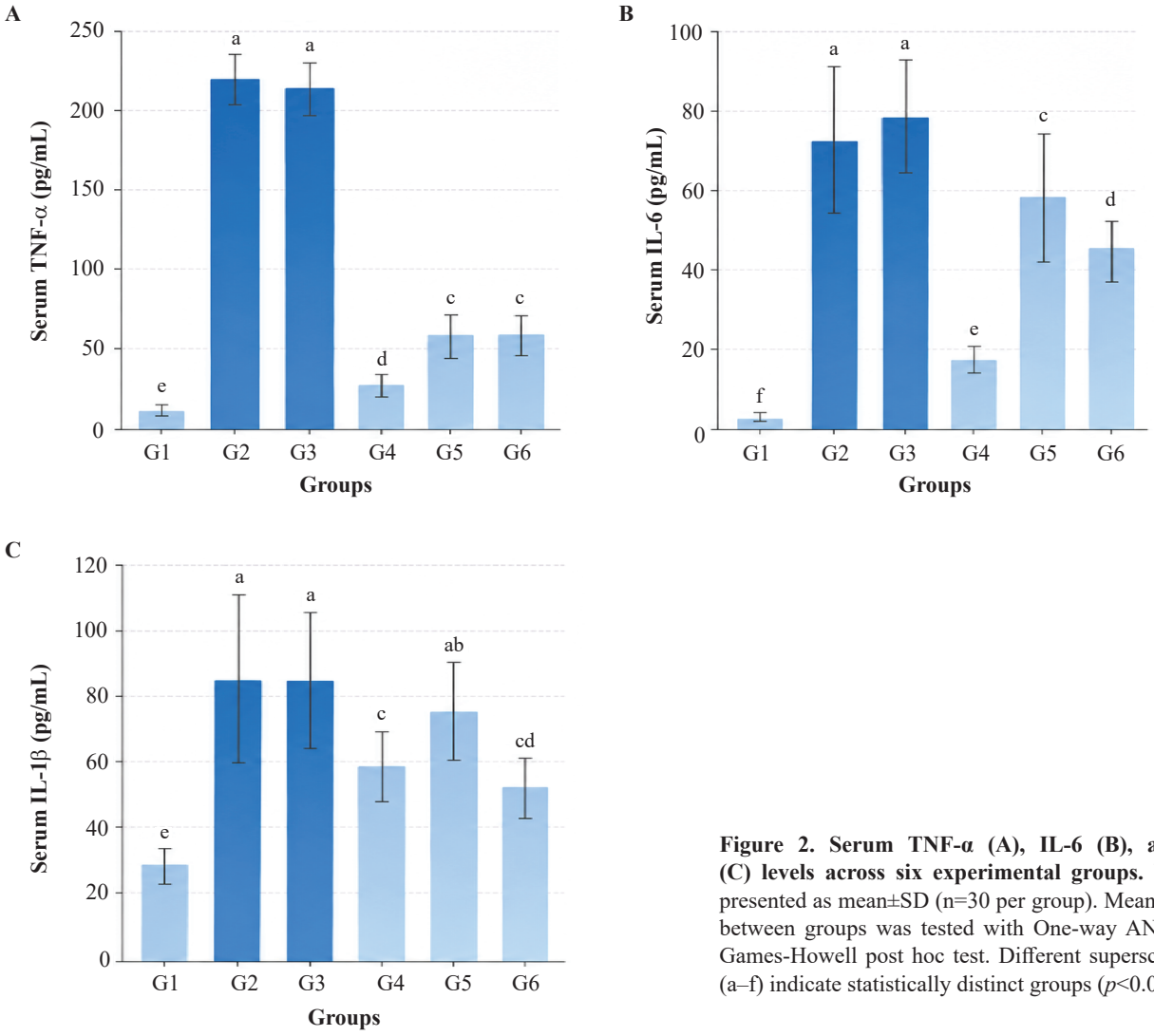


Figure 2. Serum TNF-α (A), IL-6 (B), and IL-1β (C) levels across six experimental groups. Values are presented as mean±SD (n=30 per group). Mean difference between groups was tested with One-way ANOVA with Games-Howell post hoc test. Different superscript letters (a–f) indicate statistically distinct groups (p<0.05).

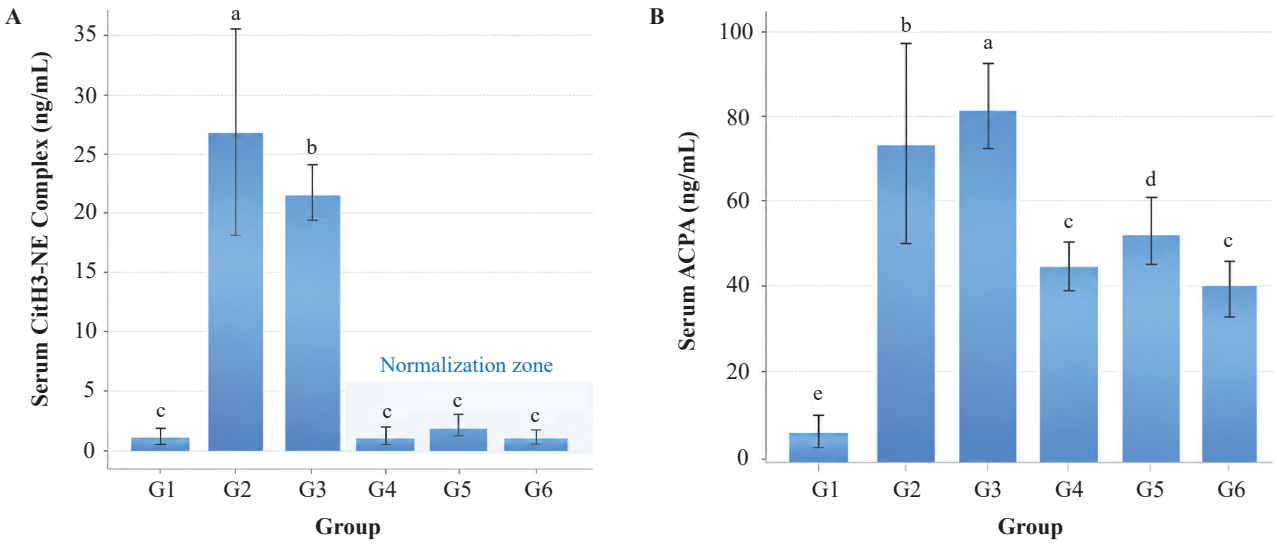


Figure 3. Serum Cit H3-NE complex (A) and ACPA (B) levels across six experimental groups. Light blue shaded zone (in A) marked complete CitH3-NE normalisation in all treatment groups. Values are presented as mean±SD (n=30 per group). Mean difference between groups was tested with One-way ANOVA with Games-Howell post hoc test. Different superscript letters (a–f) indicate statistically distinct groups (p<0.05).

followed by Games–Howell post hoc test to indicate which groups have statistically significant differences.

The same trend was observed within groups. The highest concentrations of nucleic acid complexes, pro-inflammatory cytokines, and autoantibodies are found in the disease groups (G2 and G3), which mostly carry the superscript letter "a" for the majority of inflammatory markers, including IL-6, IL-1β, TNF-α, and MPO-DNA. These results illustrate a robust inflammatory and autoimmune response at the peak and the sustained phases of the disease model. The healthy control group (G1) shows the lowest biomarker levels and is typified by the lowest statistical classifications (*e.g.*, "e" and "f"), which represent baseline healthy conditions.

The treatment groups (G4, G5, and G6) show moderate biomarker levels with substantial decreases compared to the untreated disease groups. Their statistical distribution within intermediate superscripts (*e.g.*, "c" and "d") indicates partial restoration toward normal physiological status. In general, the table demonstrates a well-structured separation between healthy, diseased, and treated conditions, showing the significant modulatory effects of the tested interventions on inflammatory and autoimmune biomarker profiles.

Pearson Correlation Network: Disease Phase Groups (G1–G3)

In G1, no statistically significant correlations were detected, confirming physiological homeostasis. G2 revealed a highly integrated positive correlation network: NE ↔ CitH3 (r=0.69, p<0.001), MPO ↔ IL-6 (r=0.66, p<0.001), and CitH3 ↔ ACPA (r=0.66, p<0.001). G3 demonstrated the strongest study-wide correlation: IL-6 ↔ ACPA (r=0.74, p<0.001), quantitatively demonstrating NET–ACPA–IL-6 loop entrenchment in chronic CIA (Table 3). The NE–CitH3 correlation disappeared from G2 (r=0.69) to G3 (r=0.19, p=0.316) despite sustained CitH3-NE elevation, indicating a mechanistic transition from NE-driven acute NETosis to cytokine-receptor-driven chronic PAD4.

Figure 4 shows Pearson correlation networks for the measured physiological and developmental parameters across three experimental conditions: baseline control without ventilation correlations, a 30-minutes interval integrated ventilation network, and a 60-minutes interval integrated ventilation network. In the baseline condition, most variables exhibited weak to moderate positive correlations. The strongest were found between CEJ-3 and M-7L (r=0.48) and between Z6-A+α and CEJ-3 (r=0.42). After the 30-minutes interval ventilation strategy was introduced, correlation strengths rose markedly throughout the 30-minutes interval integrated ventilation network, suggesting greater synchronization among the measured parameters. Strong positive associations appeared between CEJ-3 and M-7L (r=0.78), E-6-0 and Z6-A+α (r=0.67), and E-4-1 and E-6-0 (r=0.63). The 60-minutes interval strategy generated the strongest network overall, with very high positive relationships across multiple variables. The strongest correlations appeared between CEJ-3 and M-7L (r=0.93), followed by Z6-A+α with CEJ-3 (r=0.89) and

Table 3. Mechanistic interpretations were restricted to Pearson correlations that achieved statistical significance.

Group	Biomarker Pair	r (*p*-value)	Mechanistic Interpretation	Significancy
G2	NE ↔ Cit H3	r=0.69 (p<0.001)	NE-PAD4 co-activation in acute suicidal NETosis	**
G2	MPO ↔ IL-6	r=0.66 (p< 0.001)	MPO oxidative burst drives macrophage IL-6 activation	**
G2	Cit H3 ↔ ACPA	r=0.66 (p<0.001)	Citrullinated histones as primary ACPA autoantigens	**
G3	IL-6 ↔ ACPA	r=0.74 (p<0.001)	Strongest study-wide: NET–ACPA–IL-6 loop entrenchment	**
G3	Cit H3 ↔ ACPA	r=0.64 (p<0.001)	Persistent citrullinated antigen-driven ACPA production	**
G4	NE ↔ Cit H3	r=0.42 (p=0.021)	Attenuated: dual MPO/PAD4 decoupling	*
G5	MPO ↔ ACPA	r=0.51 (p=0.004)	Retained: residual oxidative citrullinated antigen generation	**
G6	Cit H3 ↔ ACPA	r=0.59 (p=0.001)	Retained: residual PAD2-mediated citrullination	**

Only statistically significant Pearson correlations (p<0.05) are presented. Pearson's correlation coefficient (r) represents the strength and direction of the association between the indicated biomarker pairs; *p< 0.05; **p<0.01. Non-significant correlations were omitted, therefore, interpretations regarding the association between IL-6 and ACPA were only dropped from the groups in which this association did not reach statistical significance.

E-6-0 with Z6-A+α (r=0.86). This pattern suggests that lengthening the ventilation interval increased interaction and coordination among the physiological and developmental indicators, producing a more integrated network structure than the baseline condition.

Pearson Correlation Network: Treatment Groups (G4–G6)

G4 achieved the most comprehensive network dismantling: NE ↔ CitH3 attenuated to r=0.42 (p=0.021), and the IL-6 ↔ ACPA correlation was completely abolished (r=0.30, p=0.103). G5 demonstrated retained MPO ↔ ACPA (r=0.51, p=0.004) and MPO ↔ NE (r=0.53, p=0.003), indicating residual MPO activity continuing to drive citrullinated antigen generation. G6 demonstrated a PAD4-selective fingerprint with retained CitH3 ↔ ACPA (r=0.59, p=0.001), indicating residual PAD2-mediated citrullination under selective PAD4 blockade (Figure 5). Key correlations across all groups are summarised in Table 3.

Fluorescence Microscopy: Four-Stage NETosis Classification

Direct visual validation was provided by SYTOX Green fluorescence microscopy of synovial lavage fluid (Figure 6). G1 demonstrated a complete absence of extracellular DNA with fully condensed neutrophil chromatin. G2 exhibited dense web-like extracellular chromatin structures consistent with active suicidal NETosis at peak CIA. G3 demonstrated

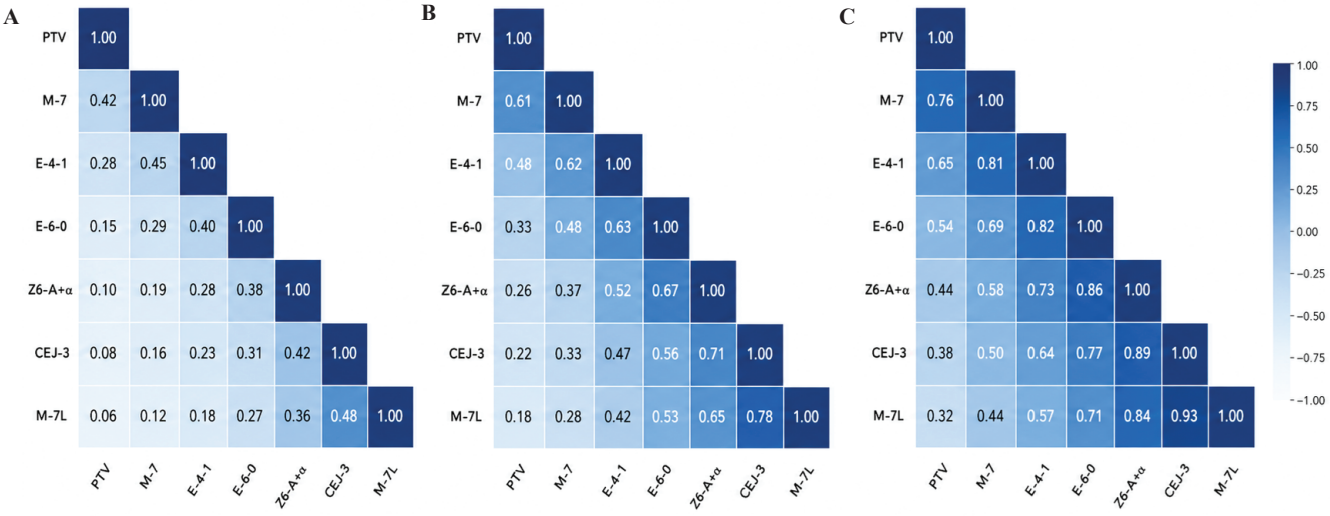


Figure 4. Pearson correlation heatmaps for disease phase groups G1–G3. A: Baseline control, no ventilation correlation. B: 30-minutes interval integrated ventilation network. C: 60-minutes interval integration loop (SN-T/ZONE-6A). Lower triangular matrices display Pearson r values. Colour scale: dark blue = strong positive (r → +1); mild or light blue = negative or absent.

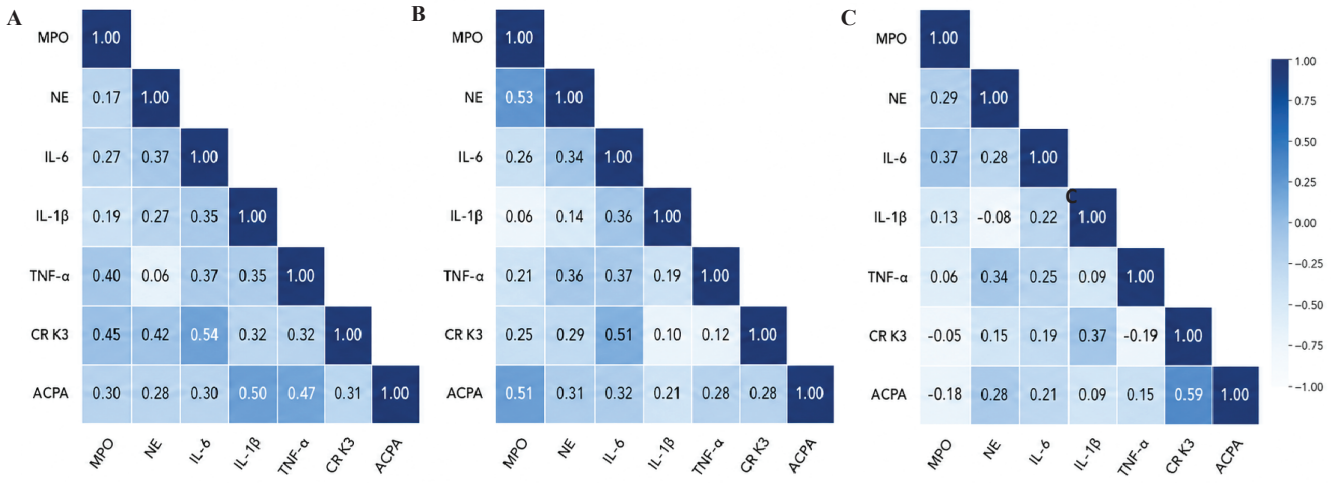


Figure 5. Pearson correlation heatmaps for treatment groups G4–G6. A: CIA + Myricetin dual-target network dismantling. B: CIA + RL6 MPO-axis retained MPO-ACPA. C: CIA + CI-amidine residual CR-K3–ACPA. Each agent demonstrates a distinct pharmacodynamic network fingerprint.

moderate scattered NET formation, confirming persistent NETosis in chronic CIA. Treatment groups (G4–G6) demonstrated markedly reduced extracellular DNA, confirming genuine NETosis abolition consistent with the biomarker normalisation data.

Discussion

This work presents the first systematic Pearson Correlation Network analysis of the NET–ACPA–IL-6 autoimmune amplification loop in CIA, tracking its progressive development across disease phases and differential pharmacological disruption by three mechanistically distinct agents.(19,20) The study provides four principal findings: measurable amplification of the autoimmune loop at a rate of 0.34 ng/mL ACPA/day in untreated chronic CIA; IL-6–ACPA correlation strength (r=0.74) that quantitatively reflects entrenchment of the loop; distinct pharmacological routes to complete normalization of CitH3-NE, converging on PAD4 as a rate-limiting regulatory node; and each intervention unveils residual pathway activity invisible to single-biomarker assessment with a unique pharmacodynamic fingerprint.(21,22,23)

The increase in ACPA is quantified evidence of epitope spreading and early ACPA expansion before the onset

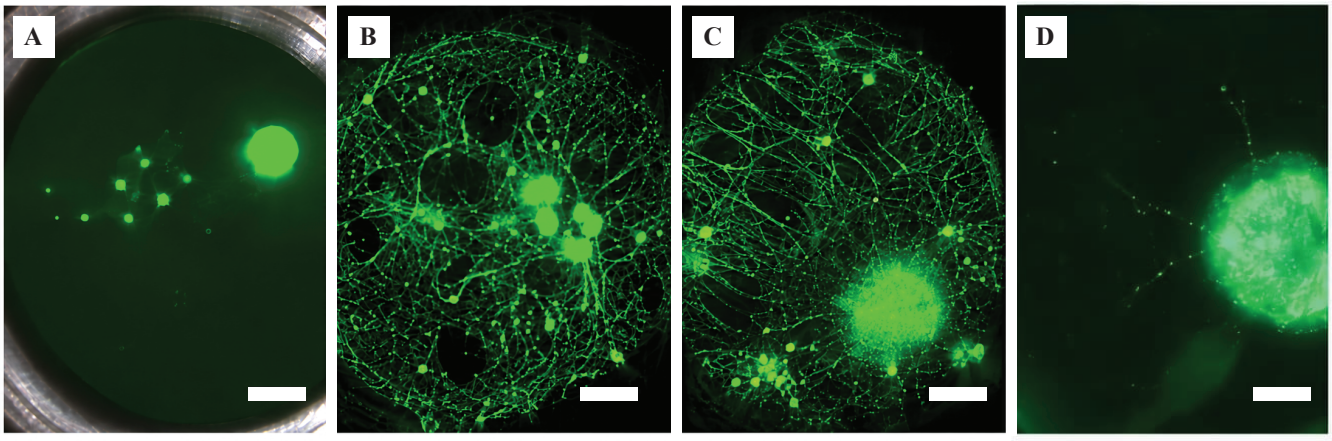


Figure 6. Fluorescence microscopy of synovial lavage fluid with SYTOX green staining (500 nM; excitation/emission 488/523 nm). A: G1 (healthy control): Intact condensed chromatin, no NETosis. B: G2 (acute CIA): Dense web-like NET structures, advanced NETosis. C: G3 (chronic untreated CIA): Scattered extracellular chromatin, moderate persistent NETosis. D: G4–G6 (treatment groups): Near-complete chromatin condensation,NETosis suppressed. White bar: 50 μm.

of rheumatoid arthritis, as observed in the clinic.(24,25) Longitudinal studies on RA further validate the fact that ACPA levels predict disease progression and radiographic outcomes, and the clinical aspects of ACPA kinetics are relevant.(21) The IL-6–ACPA correlation strengthens from G2 to G3, suggesting a bidirectional mechanistic axis. IL-6 triggers the differentiation of plasma cells dependent on Tfh through JAK1/STAT3/IL-21 signalling, whereas ACPA-containing immune complexes trigger neutrophil activation and NET formation.(12,13) Intra-articular NETs are correlated with IL-6 in autoimmune arthritis, thus reinforcing the amplification loop between NETs and cytokines.(21) ACPA-containing IgG induces NETosis directly; NET products then enhance IL-6 production.(15) Besides, synovial B cells in the joints of RA patients further boost the production of antibodies against citrullinated NET histones, thus reinforcing the autoimmune loop.(23) This further supports the pivotal role of IL-6 in disease perpetuation since in RA patients, clinical associations of IL-6 with disease activity and cardiovascular risk have been reported.(26) The observed dissociation of NE–CitH3 correlation from acute to chronic disease indicates a switch from neutrophil-driven NETosis to cytokine- and PAD4-driven chronic amplification, in line with sustained feedback inflammatory mechanisms.

Differences in MPO-DNA and NE-DNA responses will further delineate the mechanistic steps in NET formation. CI-Amidine showed better NE-DNA reduction over RL6, indicating that PAD4-mediated chromatin decondensation is a step above MPO inhibition as a rate-limiting step in NETosis. While MPO is required for NETosis and its inhibition decreases inflammatory and arthritic outcomes (as discussed earlier), these data show that PAD4 has a broader effect on downstream NET structural components. Myricetin, a dual MPO/PADI4 inhibitor, suppressed both pathways at the same time, in keeping with its reported anti-NETotic effects. RA-derived neutrophil subsets have been reported to have enhanced NETosis potential (19), providing a biological explanation for the exaggerated responses observed in CIA.

The Normalization of CitH3-NE across all treatments further places PAD4 as a primary convergence node in the regulation of NETosis. Since genetic deficiency abolishes NETosis irrespective of the upstream stimuli, this finding further solidifies the role of PAD4 as critical for NET formation. As the inhibitor of PAD4 has been developed extensively and there is emerging clinical translation, including dual PAD-targeting strategies, this finding further supports its role as a therapeutic target. The observed suppression below the physiological baseline in the Myricetin group (G3) hints at potential basal PAD4 activity and therefore calls for dose-optimisation studies.

Even though CitH3-NE levels were similar, the different IL-1β responses indicate that some NETs do not stop producing the cytokines once their structure is cleared. High IL-1β in the RL6 group (G5) may be due to some NLRP3 activation by immune complexes that remained after the NETs were cleared. This is because PAD4 inhibits the activation of NLRP3.(27) IL-1β can be sustained directly by ACPA-holding immune complexes.(28,29) Myricetin also worked anti-inflammatory in a broad sense, reducing TNF-α through multiple pathways.(30) Thus demonstrating its pleiotropic mechanism.

In total, three agents had pharmacodynamic fingerprints that were different: Myricetin was a general suppressor of the IL-6-ACPA axis; RL6 mainly reduced the MPO-driven oxidative NET pathways; and CI-Amidine targeted PAD4-dependent structural NET formation with some residual cytokine signalling. These profiles complement each other and suggest rational combination strategies for complete disruption of NET-associated autoimmune networks. Most importantly, MPO-DNA, NE-DNA, and Cit H3 were very good pharmacodynamic biomarkers, better than single-marker evaluation (31), and thus validate the correlation-network approach used in the present study. The central role of NETs in autoimmune amplification across diseases further underlines the translational relevance of this framework (10,11).

Also, the observed regulation of IL-6 suggests likely downstream effects on Th17/Treg balance since it has been established that NETs can support Th17 polarisation and autoimmune persistence.(32-34) Histones and citrullinated peptides from NETs also sustain T-cell activation; thus, by reducing PAD4 activity, autoantigen availability may be diminished, and immune priming inhibited.(35-37) Because such biomarkers have been correlated with clinical RA indices , the current seven-marker panel can probably be a translational pharmacodynamic platform for anti-NETotic clinical trials in the future.(38-40)

Conclusion

This study shows that the NET-ACPA-IL-6 network is a dynamic autoimmune amplification system in CIA model and can be effectively modulated by pharmacological intervention. All tested treatments attenuated key components of this pathogenic network and reduced biomarkers

associated with NETosis and inflammation. Correlation network analysis further revealed distinct treatment-specific effects on biomarker interactions, highlighting differences in their mechanisms of action. These results thus validate the NET-ACPA-IL-6 axis as a promising pharmacodynamic framework and a potential therapeutic target in RA.

Acknowledgments

The authors gratefully acknowledge the institutional animal facility staff and laboratory personnel for their technical assistance throughout this study.

Authors Contribution

ASH contributed to all research requirements, including writing, laboratory work, interpretation, and analysis of results, while WSS supervised the research and contributed to editing and revising the manuscript.

Ethical Statement

All animal experimental procedures were carried out in conformity with the guidelines for the care and use of laboratory animals and approved by the Research Ethics Committee of the University of Basrah, Basrah, Iraq. Ethical approval was obtained under approval No. REC-2026-555 on January 6, 2026.

Conflict of Interest

The authors declare no conflicts of interest.

References

1. Sparks JA. Rheumatoid arthritis. Ann Intern Med. 2019; 170(1): ITC1-ITC16. doi: 10.7326/AITC201901010.
2. McInnes IB, Schett G. The pathogenesis of rheumatoid arthritis. N Engl J Med. 2011; 365(23): 2205-19.
3. Smolen JS, Aletaha D, McInnes IB. Rheumatoid arthritis. Lancet. 2016; 388(10055): 2023-38.
4. Kaplan MJ, Radic M. Neutrophil extracellular traps: Double-edged swords of innate immunity. J Immunol. 2012; 189(6): 2689-95.
5. O'Neil LJ, Kaplan MJ. Neutrophils in rheumatoid arthritis: Breaking immune tolerance and fueling disease. Trends Mol Med. 2019; 25(3): 215-27.
6. Nielen MM, van Schaardenburg D, Reesink HW, van de Stadt RJ, van der Horst-Bruinsma IE, de Koning MH, *et al.* Specific autoantibodies precede the symptoms of rheumatoid arthritis: A study of serial measurements in blood donors. Arthritis Rheum. 2004; 50(2): 380-6.
7. van Delft MAM, Huizinga TWJ. An overview of autoantibodies in rheumatoid arthritis. J Autoimmun. 2020; 110: 102392. doi: 10.1016/j.jaut.2019.102392.
8. Brinkmann V, Reichard U, Goosmann C, Fauler B, Uhlemann Y, Weiss DS, *et al.* Neutrophil extracellular traps kill bacteria. Science. 2004; 303(5663): 1532-5.
9. Papayannopoulos V. Neutrophil extracellular traps in immunity and disease. Nat Rev Immunol. 2018; 18(2): 134-47.
10. Fousert E, Toes R, Desai J. Neutrophil extracellular traps (NETs) take the central stage in driving autoimmune responses in infectious diseases. Cells. 2020; 9(4): 915. doi: 10.3390/cells9040915.
11. Apel F, Zychlinsky A, Kenny EF. The role of neutrophil extracellular traps in rheumatoid arthritis. Front Immunol. 2023; 14: 1160793. doi: 10.3389/fimmu.2023.1160793.
12. Mao CL, Yu CH, Jiang SL, Ying ZH, Zhu XY. Neutrophil extracellular traps in rheumatoid arthritis: Pathogenic mechanisms and therapeutic potential. Front Immunol. 2025; 16: 1717671. doi: 10.3389/fimmu.2025.1717671.
13. Kumari S, Pardali K, Kraan M, Meldrum E, Lood C. Neutrophil extracellular traps in rheumatoid arthritis: Biomarkers, drivers, and emerging therapeutic targets. Clin Exp Immunol. 2026; 220(1): uxag011. doi: 10.1093/cei/uxag011.
14. Khandpur R, Carmona-Rivera C, Vivekanandan-Giri A, Gizinski A, Yalavarthi S, Knight JS, *et al.* NETs are a source of citrullinated autoantigens and stimulate inflammatory responses in rheumatoid arthritis. Sci Transl Med. 2013; 5(178): 178ra40. doi: 10.1126/scitranslmed.3005580.
15. Wu W, Wang W, Liu J, Cheng L, Li N. Anti-citrullinated protein antibodies are associated with neutrophil extracellular trap formation in rheumatoid arthritis. J Clin Lab Anal. 2021; 35(3): e23662. doi: 10.1002/jcla.23662.
16. Shu Y, Yang R, Wen H, Dong Q, Chen Z, Xiang Y, *et al.* Myricetin reduces neutrophil extracellular trap release in a rat model of rheumatoid arthritis, which is associated with a decrease in disease severity. Innate Immun. 2024; 30(2-4): 66-78.
17. Matos IA, Dallazen JL, Reis LR, de Moura RD, Ronsein GE, Hoch NC, *et al*. Targeting myeloperoxidase ameliorates gouty arthritis: A virtual screening success story. J Med Chem. 2024; 67(15): 12987-3003.
18. Willis VC, Gizinski AM, Banda NK, Causey CP, Knuckley B, Cordova KN, *et al.* N-α-benzoyl-N5-(2-chloro-1-iminoethyl)-L-ornithine amide, a protein arginine deiminase inhibitor, reduces the severity of murine collagen-induced arthritis. J Immunol. 2011; 186(7): 4396-404.
19. Denny MF, Yalavarthi S, Zhao W, Thacker SG, Anderson M, Sandy AR, *et al*. J. A distinct subset of proinflammatory neutrophils isolated from patients with systemic lupus erythematosus induces vascular damage and synthesizes type I IFNs. J Immunol. 2010; 184(6): 3284-97.
20. Metzler KD, Fuchs TA, Nauseef WM, Reumaux D, Roesler J, Schulze I, Herrmann M, Zychlinsky A, Kettritz R. Myeloperoxidase is required for neutrophil extracellular trap formation: Implications for innate immunity. Blood. 2011; 117(3): 953-9.
21. Hashizume M, Yoshida H, Koike N, Suzuki M, Mihara M. Specific increase in joint neutrophil extracellular traps and its relation to interleukin-6 in autoimmune arthritis. Front Immunol. 2021; 12:

644365. doi: 10.3389/fimmu.2021.644365.
22. Spengler J, Beller E, Leffler J, Blom AM, Moll S, Carmona A, *et al.* ACPA in early inflammatory arthritis. Rheumatology. 2015; 54(8): 1400-8.
23. Corsiero E, Bombardieri M, Carlotti E, Pratesi F, Robinson W, Migliorini P, *et al.* Single cell cloning and recombinant monoclonal antibodies generation from RA synovial B cells reveal frequent targeting of citrullinated histones of NETs. Ann Rheum Dis. 2016; 75(10): 1866-75.
24. Deane KD, Holers VM, Bemis EA. Rheumatoid arthritis: The continuum of disease and strategies for prediction, early intervention and prevention. J Rheumatol. 2024; 51(4): 337-49.
25. Soyfoo MS, Sarrand J. Multi-marker panels for the diagnosis and disease activity monitoring of rheumatoid arthritis: A clinical immunology perspective. Diagnostics. 2026; 16(2): 330. doi: 10.3390/diagnostics16020330.
26. Roghani SA, Shamsi A, Jalili C, Jalili F, Lotfi R, Garman N, *et al.* Interleukin-6 positively correlates with cardiovascular disease predictor algorithms and biomarkers in rheumatoid arthritis patients. J Cell Mol Med. 2024; 28(17): e70028. doi: 10.1111/jcmm.70028.
27. Almatroodi SA, Rahmani AH. Myricetin and its therapeutic potential in inflammatory and autoimmune diseases: A comprehensive pharmacological review. Int J Mol Sci. 2025; 26(9): 4188. doi: 10.3390/ijms26094188.
28. Dong X, Sun Q, Wei Y. ACPA-positive IgG activates the NLRP3 inflammasome and induces IL-1β production through FcγRIIA in human neutrophils. Cell Mol Immunol. 2019; 16(1): 72-85.
29. Ruscitti P, Cipriani P, Giacomelli R. NLRP3 inflammasome in rheumatoid arthritis: Structural and functional contributions to joint inflammation, bone erosion and therapeutic opportunity. Int J Mol Sci. 2024; 25(6): 3202. doi: 10.3390/ijms25063202.
30. Jose AM, Samarpita S, Panchal NK, Sabina EP, Rasool M. Myricetin selectively binds IL-21 and inhibits IL-21/IL-21R interaction, suppressing T-follicular-helper cell differentiation in adjuvant-induced arthritis via the JAK/STAT3/Bcl-6 axis. 3 Biotech. 2024; 14(1): 25. doi: 10.1007/s13205-023-03896-8.
31. Melamud MM, Tolmacheva AS, Sizikov AE, Klyaus NA, Zhuravlev ES, Stepanov GA, *et al.* NETosis-related biomarkers in systemic lupus erythematosus, rheumatoid arthritis, psoriatic arthritis and ankylosing spondylitis: A comparative study. Int J Mol Sci. 2025; 26(24): 12127. doi: 10.3390/ijms262412127.
32. Chen J, Cao Y, Xiao J, Hong Y, Zhu Y. The emerging role of neutrophil extracellular traps in the progression of rheumatoid arthritis. Front Immunol. 2024; 15: 1438272. doi: 10.3389/fimmu.2024.1438272.
33. Bashar SJ, Shelef MA. Macrophage extracellular traps require peptidylarginine deiminase 2 and 4 and are a source of citrullinated antigens bound by rheumatoid arthritis autoantibodies. Front Immunol. 2024; 15: 1167362. doi: 10.3389/fimmu.2024.1167362.
34. Patel MM, Patel DK, Patel LB, Patel DM, Patel KJ, Patel VA, *et al.* Circulating neutrophil extracellular traps as disease severity markers for rheumatoid arthritis: A case-control study. J Lab Physicians. 2025; 17(2): 209-16.
35. Quirke AM, Lugli EB, Wegner N, Hamilton BC, Charles P, Chowdhury M, *et al.* Heightened immune response to autocitrullinated Porphyromonas gingivalis peptidylarginine deiminase: A potential mechanism for breaching immunologic tolerance in rheumatoid arthritis. Ann Rheum Dis. 2016; 75(5): 985-93.
36. Tang J, Xia J, Gao H, Jiang R, Xiao L, Sheng H, *et al.* IL-33-induced neutrophil extracellular traps mediate a positive feedback loop for synovial inflammation and NET amplification in rheumatoid arthritis. Exp Mol Med. 2024; 56(12): 2602-16.
37. Thiam HR, Wong SL, Wagner DD, Bhatt DL. Molecular mechanisms of NETosis in inflammatory diseases. Proc Natl Acad Sci USA. 2020; 117(41): 25257-65.
38. Tillack K, Breiden P, Martin R, Sospedra M. T lymphocyte priming by neutrophil extracellular traps links innate and adaptive immune responses. J Immunol. 2012; 188(7): 3150-9.
39. Velásquez EA, Torres-Aguilar H, González-Amaro R. Peptidylarginine deiminase inhibitors in autoimmune disease: Current status and therapeutic perspectives for PAD2/PAD4 selective and bispecific targeting. Int J Mol Sci. 2025; 26(5): 2187. doi: 10.3390/ijms26052187.
40. Wright HL, Lyon M, Chapman EA, Moots RJ, Edwards SW. Rheumatoid arthritis synovial fluid neutrophils drive inflammation through production of chemokines, reactive oxygen species, and neutrophil extracellular traps. Front Immunol. 2020; 11: 584116. doi: 10.3389/fimmu.2020.584116.